Deuterium plasma exposure of rhodium films: role of morphology and crystal structure

A Uccello[1], B Eren[2], L Marot[2], D Dellasega[1,3], A Maffini[1], R Steiner[2], D Mathys[4], E Meyer[2] and M Passoni[1,3]

[1] Dipartimento di Energia, Politecnico di Milano, Italy
[2] Department of Physics, University of Basel, Klingelbergstrasse 82, CH-4056 Basel, Switzerland
[3] Istituto di Fisica del Plasma, Consiglio Nazionale delle Ricerche, EURATOM-ENEA-CNR Association, Milan, Italy
[4] Centre of Microscopy, University of Basel, Klingelbergstrasse 50/70, CH-4056 Basel, Switzerland

E-mail: andrea.uccello@polimi.it

Abstract. The behaviour of rhodium film mirrors with different crystal structure and morphology toward a deuterium plasma is presented. The specular reflectivity of rhodium films was monitored before, during and after exposure. To understand the reflectivity behaviour of the rhodium films during exposure, samples were characterized by scanning electron microscopy, X-ray photoelectron spectroscopy and atomic force microscopy. Crystal structure and morphology of rhodium films strongly affect the change of the specular reflectivity during deuterium plasma exposure. In particular, films with few nm crystallite size and granular-like morphology prevent the reflectivity degradation, probably as a consequence of the inhibition of rhodium deuteride sub-superficial layer formation.

PACS numbers: 52.55.Fa, 28.52.Fa, 81.15.Fg, 81.07.Bc, 52.50.Qt

1. Introduction

Metallic mirrors will be crucial components of all optical systems for plasma diagnostics and imaging tools in ITER [1]. They must survive a harsh environment consisting of intense thermal loads, strong radiation fields and high particle fluxes. Two main effects of these extreme conditions are the erosion of the mirror surface by charge exchange neutrals and the re-deposition of the sputtered material transported from the first wall onto its surface. These phenomena could lead to a dramatic decrease of the specular reflectivity of the mirror, posing a serious threat on the operation of the entire diagnostic system.

Various mirror types have been investigated so far, including polycrystalline, monocrystalline and nanostructured thin film mirrors [2]. The former choice appears to be the simplest solution in terms of cost and availability of the production techniques.

However polycrystalline mirrors develop a complex step relief pattern when eroded by an ITER-relevant plasma [3, 4]. This behaviour has been attributed to the difference of the sputtering yield of grains oriented differently with respect to the surface. A monocrystal mirror or a mirror composed of crystallites with nanometric size should guarantee a more uniform erosion during tokamak operation (the surface relief pattern maintains small with respect to the wavelength of the reflected light, thus ensuring a low diffuse reflectivity) and ultimately a more reliable diagnostic system. Since both high production costs and technical difficulties prevent the manufacture of monocrystalline mirrors with diameters larger than 10 cm, thin film technologies can offer a cheaper and feasible solution for ITER scientists and engineers.

One of the principal materials considered for the production of thin film mirrors is rhodium (Rh), thanks to its high reflectivity in a wide wavelength range and acceptable sputtering yield. Recently, two techniques have been exploited to produce nanostructured Rh film mirrors: magnetron sputtering [5, 6] and pulsed laser deposition (PLD) [7, 8]. The former permits to obtain planar films on large and complex shaped areas and first mock-ups have already been produced [9], whereas the latter guarantees a detailed control on both morphology and nanostructure of the deposited films. Exploiting these techniques, it is possible to obtain films with a great variety of morphologies and crystal structures, in terms of crystallographic orientation and crystallite size (i.e. the sub-grains dimension measured by X-ray diffractometer) from a few nanometers to $\sim$30 nm. A major open issue is the behaviour of Rh film mirrors in erosion dominated zones as a function of their morphology and crystal structure.

In this work, four Rh film mirrors with different morphologies and crystal structures were produced by magnetron sputtering and PLD, and exposed to a laboratory deuterium plasma. Such an approach permits to conduce a dedicated *in situ* analysis of the physical problem of mirrors under erosion during tokamak operation. The specular reflectivity of the rhodium films was measured both before and after plasma exposure by a spectrophotometer and was monitored during the exposure by an *in situ* reflectometry system [10]. In order to understand the changes in the reflectivity of the Rh films under deuterium ions bombardment, the samples were characterized by scanning electron microscopy (SEM), atomic force microscopy (AFM) and X-ray photoelectron spectroscopy (XPS).

In section 2, the preparation methods of the Rh films, the deuterium plasma exposure facility and the characterization techniques are presented. The experimental results, focused on the effect of the deuterium plasma exposure of Rh films on their optical properties, morphology changes, and chemical composition, are shown in section 3 and discussed in section 4. Concluding remarks are presented in section 5.

2. Experimental

One Rh film was produced by the magnetron sputtering technique, while three films by the PLD method. The latter were deposited in different experimental conditions

in order to obtain various morphologies and crystallite size. All the samples were deposited on stainless steel-316L (SS) substrates (25 mm diameter, 2 mm thick) which were mechanically polished (first by abrasive SiC paper, then by diamond paste, and finally by an alumina powder of 0.05 μm particle size).

Details about the complete deposition procedure and characterizations of the magnetron sputtered Rh film, henceforth referred to as "MS", are given in [5, 6]. In summary, the average crystallite size was around 10 nm, the crystallites did not show any specific texture or preferential orientation and SEM cross-section analysis revealed dense columnar structure.

The production method of the PLD Rh films is described in [8]. The first PLD Rh coating was deposited in high-vacuum (3×10^{-3} Pa) and is labeled as "columnar" in the rest of the text, because its SEM cross-section reveals a columnar structure [8]. The deposition of the second and the third kind of samples, labeled as "NC1" ("NC" stands for nanocrystalline) and "NC2", was performed in helium atmosphere at 40 Pa and 55 Pa, respectively. The laser fluence and the distance between the target and the substrate were fixed to 10 J/cm^2 and 70 mm. In order to guarantee a high mechanical stability for NC1 and NC2 coatings, a Rh columnar adhesion layer was deposited directly above the stainless steel substrate [8]. To investigate the crystallite size and orientation of the PLD Rh films, they were characterized by X-ray diffraction (XRD) using a SIEMENS D5000 instrument with monochromatic Cu Kα radiation at a glancing incidence (with different angles of the X-ray source) and using a Panalytical X'Pert Pro X-ray diffractometer with monochromatic Cu Kα radiation in $\theta/2\theta$ configuration. The mean crystallite size, estimated using the Scherrer formula from the grazing XRD spectra, for columnar, NC1 and NC2 Rh films was 12 nm, 8 nm and 6 nm, respectively. The $\theta/2\theta$ XRD spectrum revealed how the columnar sample was highly-orientated along the (111) direction. This feature, although still present, became less evident for NC1 and NC2 specimens. The ratio between the areas of peaks (111) and (200) was 217.1, 31.4 and 2.9 for columnar, NC1 and NC2 Rh films, against 2.1 for the bulk.

To investigate Rh films morphology, the four samples were analysed by a Hitachi S-4800 field emission SEM (acceleration voltage 5 kV). Figure 1 shows the SEM top-view images for MS (a), columnar (b), NC1 (c) and NC2 (d) Rh films, where compact film morphologies can be observed. In the case of the NC2 film, it is also possible to notice the presence of a slight open structure or "granular-like" morphology. Moreover, a crack network around the scratches of the polished stainless steel substrate can be observed (figure 2a). This is the result of the combination between the tensile stress present in the film and its brittle nature [8]. A typical crack width is of some tens of nanometers (figure 2b).

The details of the magnetron sputtered and the PLD samples are summarized in table 1.

The experimental setup for deuterium plasma exposure is described in detail in [10]. Deuterium plasma exposure was performed in a high-vacuum chamber [11], at a typical background pressure of 5×10^{-5} Pa. Before the exposure, Rh films were heated to a

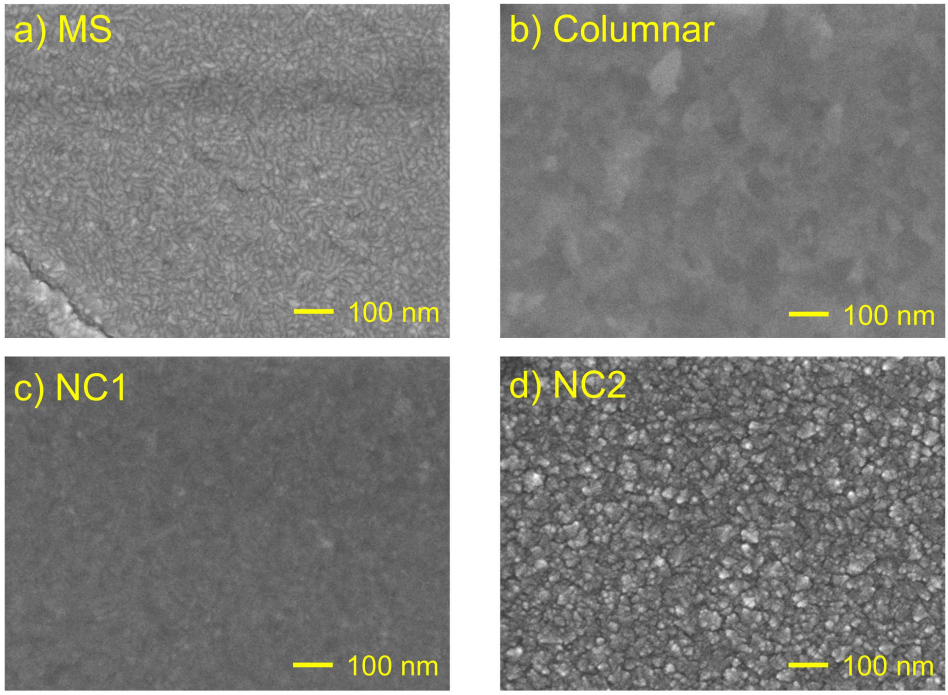

Figure 1. SEM top-view images for: MS (a), columnar (b), NC1 (c), NC2 (d) Rh films as-deposited.

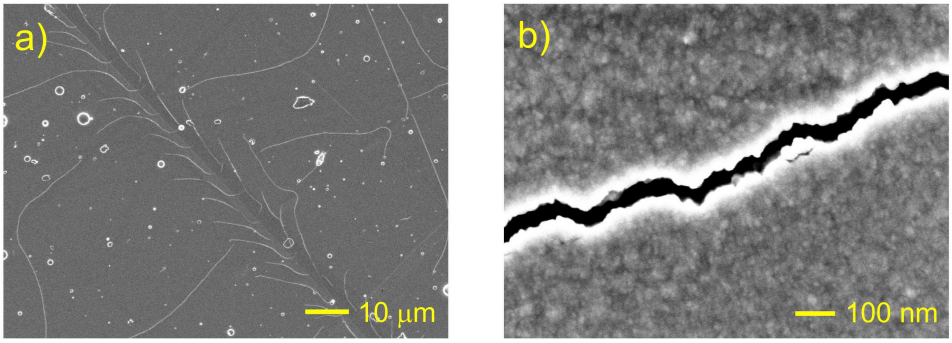

Figure 2. SEM top-view images of the NC2 Rh film at two different magnifications. (a) Crack network close to a scratch of the polished stainless steel substrate. (b) Magnified image around a crack.

temperature of 150 °C and a bias of -200 V was applied on them, in order to mimic the expected edge conditions in ITER [12]. The deuterium plasma was generated as follows: a discharge in a Pyrex tube was produced through a matching network by a 13.56 MHz radio frequency excitation at a typical power of 90 W. This excitation was coupled to the tube by an outer electrode acting as a surfatron. Deuterium was injected in the Pyrex tube with a flow of 70 sccm, in such a way that the incoming pressure was set to 3.05 Pa using conventional pumping systems. The total ions flux, including molecular ions, was estimated at 3.25×10^{15} $cm^{-2}s^{-1}$ with Langmuir probe measurements [11].

Table 1. Samples and their characteristics: deposition technique, mean crystallite size (nm) and morphology.

Sample name	Deposition technique	Mean crystallite size (nm)	Morphology
Columnar	PLD	12	no features
MS [6]	magnetron sputtering	10	no features
NC1	PLD	8	no features
NC2	PLD	6	granular-like

Ex situ UV-vis-NIR reflectivity of the mirrors was measured both before and after deuterium exposure using a Varian Cary 5 spectrophotometer equipped with a 110 mm diameter integrating sphere under nearly normal incidence ($3°20'$) in the wavelength range of 250 nm $\div$ 2500 nm, both in total and diffuse reflectivity configurations. Specular reflectivity was estimated by subtracting the diffuse reflectivity from the total reflectivity.

An *in situ* reflectometry system [10] was used to monitor the evolution of $\tilde{R}(\lambda,t)$, the specular reflectivity relative to the initial reflectivity at an incident angle of 52° at a plasma exposure time t for wavelengths λ between 400 nm and 800 nm. For the NC1 specimen, $\tilde{R}(\lambda,t)$ is available only for λ = 450 nm, 550 nm and 650 nm.

The effects of deuterium plasma on Rh films morphology were investigated by SEM and by AFM topography by means of a Veeco Thermomicroscope CP Research in non-contact mode, with scan sizes of 1, 9, 25 and 100 μm^2. The root-mean-square roughness (R_{RMS}) was then extracted from the AFM images.

Before and after plasma exposure, the samples were transferred into an ultrahigh-vacuum chamber housing a XPS, linked without breaking the vacuum to the high-vacuum exposure chamber. The electron spectrometer is equipped with a hemispherical analyzer (Leybold EA10/100 MCD) and a Mg Kα X-ray source is used (hν = 1253.6 eV) for core level spectroscopy. The typical resolution for the XPS measurements is 0.8 eV at 30 eV pass energy. The binding energy scale was calibrated using the Au $4f_{7/2}$ line of a clean gold sample at 84.0 eV. Moreover, large scale XPS spectra from 0 to 1000 eV did not reveal any other peak than those related to rhodium, oxygen and carbon. Fitting of the XPS spectra was performed using Doniach-Sunjic functions, after a Shirley background substraction with the help of UNIFIT 2011 software. A convolution of Lorentz and Gauss line shapes was used to fit the individual peaks. Atomic concentrations were then estimated using Scofield sensitivity factors.

3. Results

Figure 3 shows the specular reflectivity measured *ex situ* before exposure as a function of the wavelength for MS (orange line), columnar (black line), NC1 (blue line) and NC2 (red line) Rh films, together with a reference (green line) calculated using optical

constants of bulk Rh [13]. Except for the NC2 morphology, Rh films specular reflectivity tends to the reference.

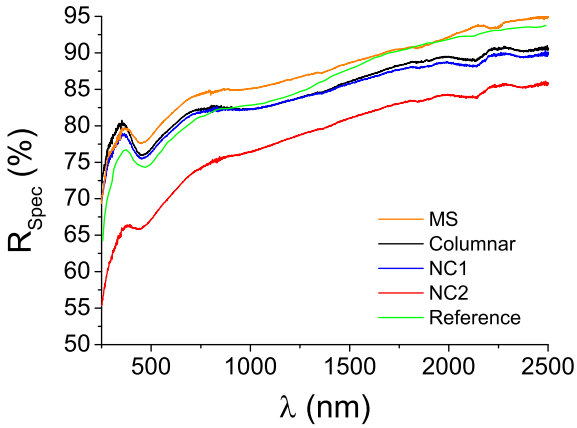

Figure 3. Specular reflectivity measured *ex situ* before the exposure as a function of the wavelength for MS (orange line), columnar (black line), NC1 (blue line) and NC2 (red line) Rh films, together with a reference (green line) calculated using optical constants of bulk Rh [13].

Figure 4 presents the behaviour of $\tilde{R}(\lambda,t)$ (see section 2) for $\lambda = 450$ nm (blue line), 550 nm (green line), 650 nm (red line) in the case of: MS (a), columnar (b), NC1 (c) and NC2 (d) Rh films. The MS film exhibited a reflectivity approximately constant during the heating and began to decrease at the plasma switch on. Both for columnar and NC1 morphologies, the heating induced a decrease in the reflectivity. At the plasma switch on there was a sharp increase of $\tilde{R}$. Finally, during the exposure it decreased. For the NC1 film, at the plasma switch off the reflectivity slowly raised. While the qualitative trend of $\tilde{R}$ was rather similar for these samples, it was very different for the NC2 morphology. In this case, both heating and plasma switch on had a beneficial effect on the reflectivity of the coating. Furthermore, $\tilde{R}$ remained rather constant during the exposure.

Figure 5 shows the difference between the specular reflectivity measured *ex situ* after and before deuterium plasma exposure as a function of the wavelength. In the case of MS, columnar and NC1 Rh films the specular reflectivity did not vary significantly after the exposure. For $\lambda < 400$ nm the spectrophotometer revealed an increase of the specular reflectivity for the MS sample (albeit it was demonstrated that this trend is not reproducible) and a decrease for the columnar and NC1 Rh films, within few percents. The specular reflectivity for the NC2 specimen increased after the exposure approximately $\sim$5% for the all wavelength range.

The effects of deuterium plasma on the Rh films morphology were investigated by SEM analysis. Figure 6 shows the SEM top-view images after the exposure for MS (a), columnar (b), NC1 (c), NC2 (d) Rh films. The MS SEM image refers to a sample which was subjected to many cycles of deuterium exposure and air storage. Comparing

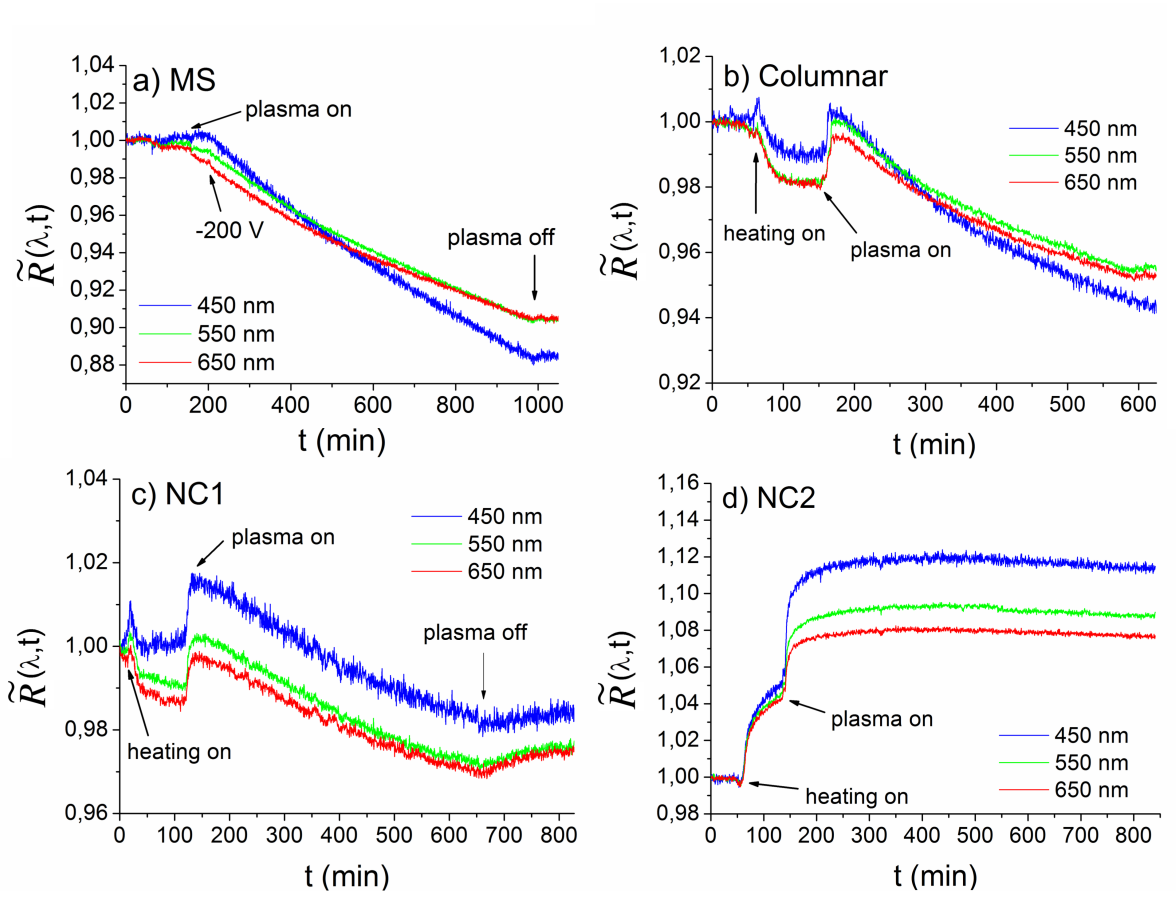

Figure 4. $\tilde{R}(\lambda,t)$ for λ = 450 nm (blue line), 550 nm (green line), 650 nm (red line) in the case of: MS (a), columnar (b), NC1 (c) and NC2 (d) Rh films. The exposure times for the Rh films were: 838 min for MS, 753 min for columnar, 533 min for NC1 and 701 min for NC2. For the columnar film the maximum value of the t-axis is 646 min because after unexpected shut-down of the *in situ* reflectometry system occurred.

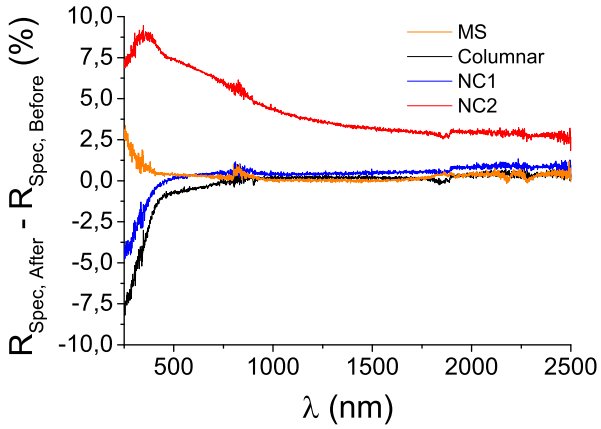

Figure 5. Difference between the specular reflectivity measured *ex situ* after and before deuterium plasma exposure as a function of the wavelength for: MS (orange line), columnar (black line), NC1 (blue line) and NC2 (red line) Rh films.

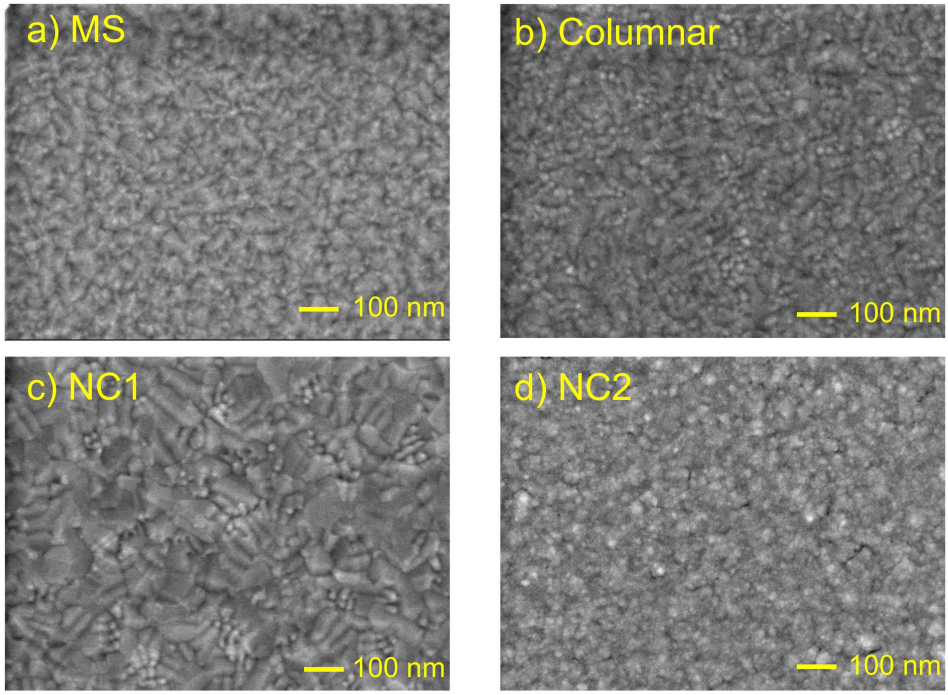

Figure 6. SEM top-view images for: MS (a), columnar (b), NC1 (c), NC2 (d) Rh films after the exposure to deuterium plasma. The MS SEM image refers to a sample which was subjected to many cycles of deuterium exposure and air storage.

figure 6 with figure 1, it is clear the change in morphology of MS, columnar and NC1 films induced by deuterium plasma. In the case of NC2 sample, the deuterium exposure did not affect the morphology as well as the crack network.

The results obtained from the XPS analyses on Rh films before and after plasma exposure, in terms of peak positions and atomic concentrations (a-C:H stands for amorphous hydrocarbons), are summarized in table 2. In the case of the MS sample, the outcomes refer to a film that was coated and measured by XPS without breaking the vacuum. It follows that no impurity peaks were observed both before and after the exposure. On the contrary, independently from the morphology, PLD Rh films (produced ex situ) were highly contaminated with oxygen and hydrocarbons before the exposure. Rh metal atomic concentration was the lowest for the NC2 specimen (35%). The exposure had a beneficial effect on the surface contamination as Rh metal atomic concentration after the process was above 90% for each PLD morphology. In particular, for the columnar film, only a metal component was present after the exposure.

4. Discussion

The results presented in section 3 show that the behaviour of Rh films under deuterium plasma exposure is significantly dependent on their crystal structure and morphology. Firstly, the lower specular reflectivity of NC2 before the exposure with respect to

Table 2. XPS analyses of the Rh films before and after deuterium plasma exposure: peak positions and atomic concentrations. BE stands for the binding energy and a-C:H for amorphous hydrocarbons.

	MS	MS exposed	Columnar	Columnar exposed	NC1	NC1 exposed	NC2	NC2 exposed
$Rh3d_{5/2}$ metal BE (eV)	307	307	307.1	307.1	307.1	307.1	307.1	307.1
$Rh3d_{5/2}$ oxide BE (eV)			308.2		307.9		307.8	
O1s 1^{st} peak BE (eV)			530.1		530.5		530.4	
O1s 2^{nd} peak BE (eV)			531.4		531.7		531.6	531.6
C1s 1^{st} peak BE (eV)			284.4		284.3	284.1	284.3	284
C1s 2^{nd} peak BE (eV)			286.3		285.2		285.4	
% Rh metal	100	100	52	100	46	93	35	92
% Rh oxide			7		9		13	
% O oxide			8		11		9	
% O			10		2		3	3
% a-C:H			23		32	7	40	5

the reference, highlighted in figure 3, could be explained in terms of a high surface contamination, as shown by XPS data in table 2. They reveal a significant amount of oxygen and hydrocarbon contaminants onto its surface (Rh metal concentration is at least ∼10% lower than that of the other configurations) [14, 15]. This hypothesis is in agreement with the granular-like feature of the NC2 film (figure 1d); such a morphology, together with the crack network (figure 2), results in a higher surface area to volume ratio with respect to the other Rh samples which could favour the percolation of water, leading to a deeper oxidation, as well as higher density of adsorption sites for hydrocarbon impurities.

The XPS data could also explain the sharp increase in reflectivity of all the PLD films at the plasma switch on, as revealed by the *in situ* reflectometry system (figures 4b-d). This phenomenon could be associated to the desorption of oxygen and hydrocarbon contaminants from the surface of the films as-deposited and also to the removal of the oxide structure for the NC2 sample.

In order to compare the effect of the deuterium plasma exposure on the *in situ* reflectivity of the different morphologies, figure 7 shows $\tilde{R}$ at $\lambda = 450$ nm, versus the total deuterium ions fluence (estimated as the product between the exposure time and the deuterium ions flux) for the different Rh films. The limit of the fluence axis is around 9×10^{19} ions cm^{-2} which corresponds to about 55 ITER discharges for mirrors in equatorial ports [16]. The trend of $\tilde{R}$ for the MS and the columnar films is quite similar. The reflectivity decrease during deuterium plasma exposure is strongly reduced for the NC1 morphology and negligible for the NC2 sample. For the PLD Rh films, it is clear that the $\tilde{R}$ decreasing rate reduces upon moving toward smaller mean crystallite sizes (see table 1).

The reflectivity decrease for MS, columnar and NC1 Rh films during deuterium plasma exposure is not due to the surface roughening of deuterium ions impact. The

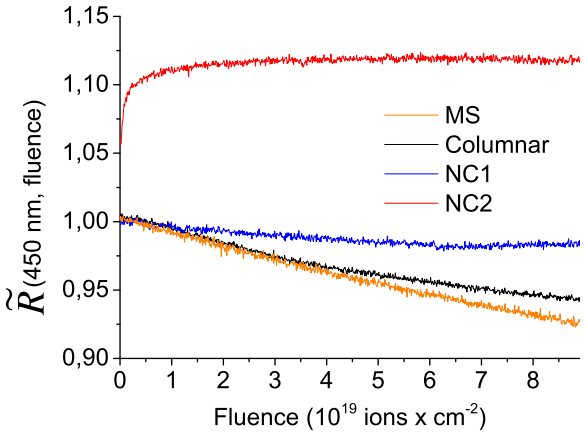

Figure 7. $\tilde{R}$, at $\lambda = 450$ nm, versus the deuterium ions fluence in the case of: MS (orange line), columnar (black line), NC1 (blue line) and NC2 (red line) Rh films.

R_{RMS} of all Rh films, evaluated from the AFM images acquired on areas of 1, 9, 25 and 100 μm^2, maintains of the order of that of the stainless steel substrate (few nanometers) even after the deuterium plasma exposure. This is consistent with the diffuse reflectivity measurements (not shown here), which exhibit values below $\sim$3% in the range of wavelength of 250 nm $\div$ 2500 nm for every Rh films both before and after the exposure.

The formation of a rhodium deuteride (RhD_x, $x \leq 2$) sub-superficial layer during deuterium plasma exposure was previously claimed to be the actual reason of the *in situ* reflectivity drop of MS, columnar and NC1 Rh films. As explained in [17], after air storage their surface got depopulated of deuterium adsorbates due to a catalytic reaction between oxygen and deuterium, which resulted in a diffusion of the incorporated deuterium first to the surface and then into air. This is consistent with the *ex situ* spectrophotometer results of figure 5 which show how the specular reflectivity of MS, columnar and NC1 Rh coatings is almost recovered for $\lambda \geq 400$ nm.

In order to stress the difference between the reflectivity measurements acquired *in situ* during plasma exposure and *ex situ* after air storage, the absolute specular reflectivity as a function of wavelength was calculated at a significant exposure time ($t = 430$ min) for each sample. To evaluate this quantity, $\tilde{R}(\lambda, t = 430 \text{ min})$ was multiplied by the specular reflectivity measured with the spectrophotometer before the exposure. Since $\tilde{R}$ was acquired at 52° while the spectrophotometer worked at a nearly normal incidence, $\tilde{R}(\lambda, t = 430 \text{ min})$ was regenerated for 0° by means of the Fresnel equations. Figure 8 summarizes the results of the analysis. The reflectivity recovery after air storage is clear for the MS and the columnar Rh films and is less significant for the NC1 specimen since its reflectivity at 430 min is still too close to that measured before the exposure. In the case of the NC2 sample, its *ex situ* specular reflectivity after deuterium plasma exposure is slightly lower than that measured *in situ* at an exposure time of 430 min. The mechanism of a rhodium deuteride sub-superficial layer formation during exposure

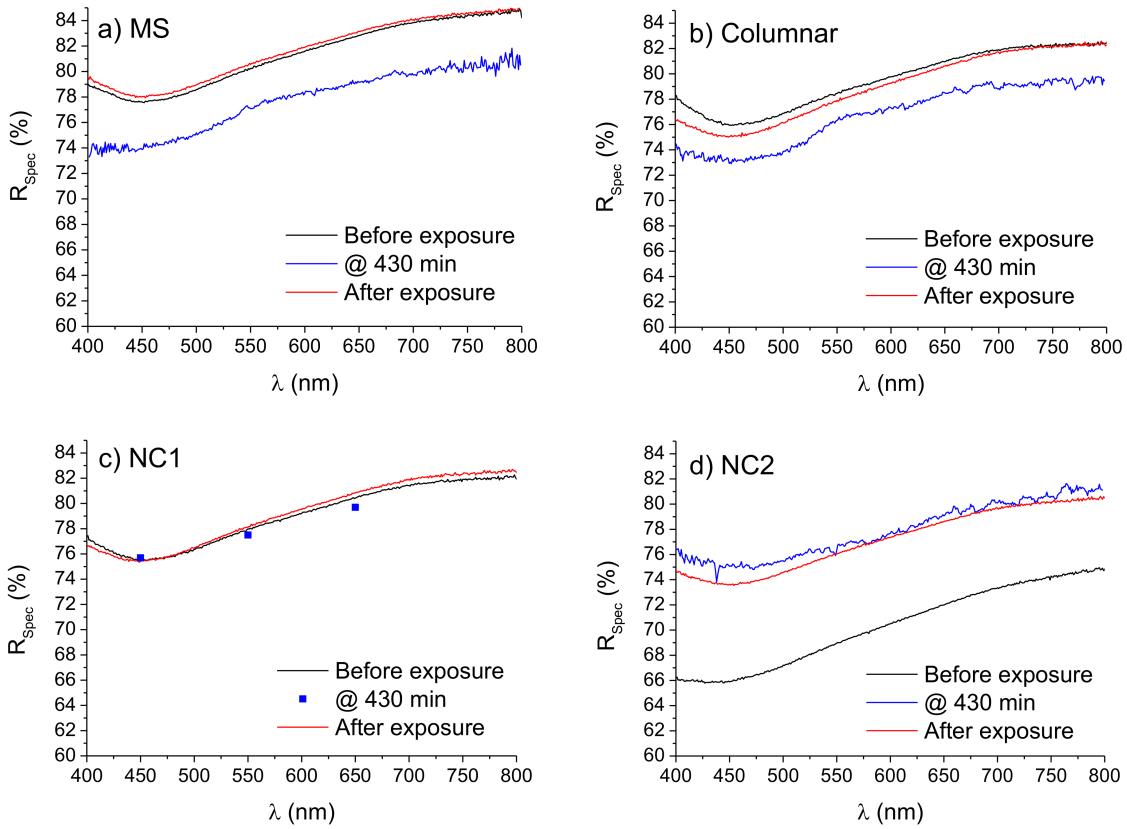

Figure 8. Specular reflectivity as a function of the wavelength measured *ex situ* before the exposure (black line), at 430 min (blue line/blue squares) and *ex situ* after the exposure (red line) for: MS (a), columnar (b), NC1 (c) and NC2 (d) Rh films. Since for the NC1 specimen $\tilde{R}(\lambda,t)$ is available only for λ = 450 nm, 550 nm and 650 nm, in figure (c) the specular reflectivity at 430 min is represented by three spots.

to the deuterium plasma potentially affected only the MS, the columnar and the NC1 Rh films, although the corresponding reflectivity decrease during exposure reduces upon moving toward smaller mean crystallite sizes. The NC2 morphology could inhibit RhD_x sub-superficial layer formation thanks to its granular-like morphology which has a high surface area to volume ratio. The implanted deuterium diffused to the pores and either was stored there or diffused out to the vacuum. The crack network also acted as further external surface for the outward diffusion. Assuming that the deuterium unloading rate of the lattice was higher than the loading one, no deuterium occupied the interstitial sites of the Rh lattice, hence the reflectivity of the NC2 sample maintained rather constant during plasma exposure. Unloading of the incorporated deuterium should also depend on the adsorption of deuterium on the Rh surface. Lower mean size of the ordered domains could influence the interaction between the Rh surface and deuterium adsorbates [18, 19], facilitating the outward diffusion. Hydrocarbon contamination could also play an additional role, since it could preoccupy deuterium adsorption sites on the

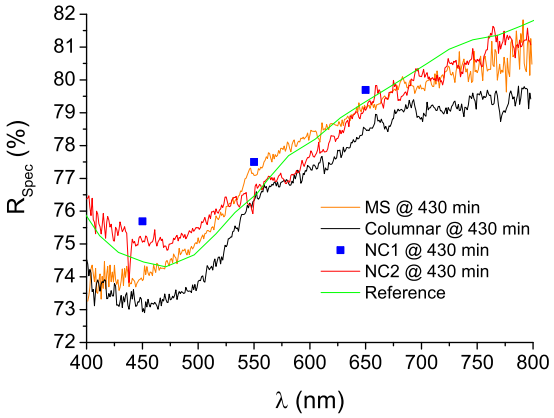

Figure 9. Specular reflectivity at 430 min for: MS (orange line), columnar (black line), NC1 (blue squares) and NC2 (red line) Rh films, together with the reference (green line).

surface. One way or another, the NC2 sample could get depopulated deuterium without requiring a reaction with oxygen. The significant tendency of the NC2 sample to adsorb contaminants explains the slight decrease of the specular reflectivity after exposure and subsequent air storage.

With the goal of estimating Rh films performance under erosion in a tokamak environment, figure 9 shows for each sample the specular reflectivity after 430 min of plasma exposure as measured by the *in situ* reflectometry system. Although the specular reflectivity of the NC2 film before the exposure was significantly lower than that of the other samples, for an exposure time of 430 min it becomes comparable with the reference. For longer exposures, the decreasing trend of $\tilde{R}$ reported in figures 4a-c for the MS, the columnar and the NC1 specimens, would bring to a specular reflectivity well below to that of the NC2 film which remains rather constant (figure 4d). Since the main requirement for a tokamak mirror is to maintain its specular reflectivity as high as possible and unchanged during operation (to make the diagnostic signal intense and reliable), the NC2 morphology shows properties suitable for use in erosion dominated zones. Exposure of the investigated Rh films in a tokamak is necessary to collect information on their performance in an environment closer to that of ITER and to obtain conclusive information toward the production of realistic mirror devices.

5. Conclusions

One magnetron sputtered Rh film and three PLD Rh coatings with different crystal structures and morphologies were exposed to a deuterium plasma to study their performance in ITER erosion dominated zones. Their specular reflectivity was monitored by an *in situ* reflectometry system during all the deuterium plasma exposure time. The reflectivity of the Rh film with a granular-like morphology and the smallest

mean crystallite size (6 nm) maintained rather constant during exposure, while a continuous degradation was observed for the other investigated configurations. This behaviour could be due to the formation of a rhodium deuteride (RhD_x, $x \leq 2$) sub-superficial layer which modified their optical properties. In the case of the Rh film with the smallest mean crystallite size, its granular-like morphology facilitated rapid outer diffusion of incorporated deuterium; thus a RhD_x layer with changed joint density of states can not be advocated anymore. As the specular reflectivity of this Rh film approached that of bulk Rh during deuterium ions bombardment and it maintained rather constant for all the exposure, it constitutes a suitable option toward the production of mirror in ITER dominated erosion zones.

Acknowledgments

The authors would like to thank G. Granucci, G. Grosso, M. Lontano for useful discussion. They thank the Swiss Federal Office of Energy and the Federal Office for Education and Science for their financial support. This work was also supported by the Swiss National Foundation (SNF), the National Center of Competence in Research on Nanoscale Science (NCCR-Nano) and the European Communities under the contract of Association EURATOM/ENEA-CNR. The views and opinions expressed herein do not necessarily reflect those of the European Commission.

References

[1] Mukhin E E, *et al* 2012 *Nucl. Fusion* **52** 013017–26
[2] Litnovsky A, Voitsenya V S, Costley A and Donné A J H 2007 *Nucl. Fusion* **47** 833–8
[3] Litnovsky A, *et al* 2007 *Fus. Eng. Design* **82** 123–32
[4] Litnovsky A, *et al* 2007 *J. Nucl. Mater.* **363–365** 1395–402
[5] Marot L, De Temmerman G, Oelhafen P, Covarel G and Litnovsky A 2007 *Rev. Sci. Instrum.* **78** 103507–13
[6] Marot L, De Temmerman G, Thommen V, Mathys D and Oelhafen P 2008 *Surf. Coat. Technol.* **202** 2837–43
[7] Passoni M, Dellasega D, Grosso G, Conti C, Ubaldi M C and Bottani C E 2010 *J. Nucl. Mater.* **404** 1–5
[8] Uccello A, Dellasega D, Perissinotto S, Lecis N and Passoni M 2013 *J. Nucl. Mater.* **432** 261–5
[9] Joanny M, Travère J M, Salasca S, Marot L, Meyer E, Thellier C, Cammarata C, Gallay G and Fermé J J 2012 *IEEE T. Plasma Sci.* **40** 692–6
[10] Wisse M, Marot L, Steiner R and Meyer E 2012 *Rev. Sci. Instrum.* **83** 013509–14
[11] Eren B, Marot L, Langer M, Steiner R, Wisse M, Mathys D and Meyer E 2011 *Nucl. Fusion* **51** 103025–34
[12] Voitsenya V S, *et al* 2001 *J. Nucl. Mater.* **290–293** 336–40
[13] Palik E D 1985 *Handbook of Optical Constants of Solids* (New York: Academic)
[14] Marot L, Mathys D, De Temmerman G and Oelhafen P 2008 *Surf. Sci.* **602** 3375–80
[15] Marot L, Steiner R, De Temmerman G and Oelhafen P 2009 *J. Nucl. Mater.* **390–391** 1135–7
[16] Matveeva M, Litnovsky A, Marot L, Eren B, Meyer E, Philipps V, Pospieszczyk A, Stoschus H, Matveev D and Samm U 21–25 June 2010 *37th EPS Conf. on Plasma Physics* (Dublin, Ireland) P2.105
[17] Eren B, Wisse M, Marot L, Steiner R and Meyer E 2013 *Appl. Surf. Sci.* **273** 94–100

[18] Vesselli E, Campaniello M, Baraldi A, Bianchettin L, Africh C, Esch F, Lizzit S and Comelli G 2008 *J. Phys. Chem.* C **112** 14475–80
[19] Mei D, Lebarbier V M, Rousseau R, Glezakou V A, Albrecht K O, Kovarik L, Flake M and Dagle R A 2013 *ACS Catal.* **3** 1133–43